Effect of trap position on the electrical properties of unipolar organic semiconductor devices

Donghyun Ko,[1] Gyuhyeon Lee,[2] Kyu-Myung Lee,[2] Yongsup Park,[2,3,*] and Jaesang Lee[1,†]
[1]*Department of Electrical and Computer Engineering, Inter-University Semiconductor Research Center, Seoul National University, Seoul 08826, Republic of Korea*
[2]*Department of Physics and Research Institute of Basic Sciences, Kyung Hee University, Seoul 02447, Republic of Korea*
[3]*Department of Information Display, Kyung Hee University, Seoul 02447, Republic of Korea*

(Received 23 October 2022; revised 7 April 2023; accepted 10 April 2023; published 26 April 2023)

We investigated the electrical properties of a unipolar organic device by intentionally inserting traps at specific positions within the device. Our findings demonstrate that the trap position has a considerable impact on the charge distribution, electric field, and charge transport behavior of the device. In particular, when the traps are positioned closer to a charge-injection electrode, the organic layer containing the traps experiences more significant band bending, resulting in a higher charge injection barrier. We propose an electrical model that fully explains the observed changes in the electrical properties of the device as a function of trap position.

DOI: 10.1103/PhysRevB.107.165204

I. INTRODUCTION

Traps are initially present or can be generated in any type of amorphous semiconductor device that is partly or entirely based on organic molecules, be it an organic light-emitting diode (OLED), an organic solar cell, an organic thin-film transistor, or even a perovskite and quantum-dot-based device [1–8]. Hence, it has long been of particular interest to researchers to understand the impact of traps because not only is their presence the inevitable nature of organics, but they also critically affect the device characteristics. For example, traps can deteriorate the optical performance of organic optoelectronic devices in which they directly quench excitons or trap free charges that are eventually removed via nonradiative recombination with the opposite charges [6,8–10]. Moreover, in order to maintain the same level of the current in a trap-containing device as that in a trap-free device, an operating voltage must be increased to supply additional free charges into the device to compensate for the trapped (or immobile) charges, which indicates an increased device resistivity.

Traps in organic devices are typically assumed to exhibit a Gaussian density of states (DOS) due to the disordered arrangement of the molecules consisting of the devices [11–13]. Several researchers have examined how the current density vs voltage (J-V) characteristics of unipolar organic devices are determined with respect to the density and energetic depth and width of the Gaussian traps [14,15]. However, the *spatial disorder of traps* and its impact on device characteristics have not been thoroughly discussed in most previous studies, despite the strong position dependence of degradation reactions, e.g., the ion migration from a metal electrode into organics [16–18] or the molecular bond dissociation induced by the highly excited states that nonuniformly occur in organic optoelectronic devices [6,19–23]. Although simulation studies have demonstrated the spatial inhomogeneity of traps in aged OLEDs [19,23], their effect on the charge and exciton dynamics, and hence the postdegradation performance, has yet to be clearly explained or experimentally investigated. The major challenge of such studies is to analytically verify the specific positions of a wide variety of traps with unknown energetics and low concentrations ($\leqslant$1wt %) and to decouple their mixed effects on device performance.

To address this challenge, we present a direct method for investigating the position-dependent J-V characteristics of a hole-only unipolar organic device (HOD) with embedded traps. Our HOD consists of a 200-nm-thick hole transport layer (HTL), within which a 5-nm-thick slab *at a specific position* is selectively doped with hole-trapping molecules at *controlled concentration* of 1 wt % and with *identified trap depth*. Our results reveal that the position of the traps has a marked impact on the distribution of holes and the electric field profile for the trap-containing HODs, leading to their distinct J-V characteristics. Specifically, the resistivity of the HODs consistently increases as the traps are moved further away from the hole-extraction electrode (cathode) and closer to the hole-injection electrode (anode) [24]. However, when the traps are located within a certain critical distance from the anode, the trend is unexpectedly reversed, meaning that the device resistivity decreases. We also observe that the trapped holes near the anode strongly influence the band bending of the HTL, thereby enhancing the energy barrier against hole injection. We considered these trap-induced band bending effects in obtaining the boundary conditions (B.C.) for the hole densities and electric potential in a J-V model, thereby accounting for the varying electrical characteristics of the HOD with respect to trap position.

II. THEORY

Kao and Hwang developed a formula to describe the trap-limited J-V characteristics of a unipolar organic device that

*parky@khu.ac.kr
†jsanglee@snu.ac.kr

 ©2023 American Physical Society

contains deep traps with the Gaussian DOS and the *spatially nonuniform* distribution. Their formula is expressed as a power law as [25,26]

$$J \propto \frac{V^{m+1}}{d_{\rm eff}^{2m+1}}, \tag{1a}$$

where

$$d_{\rm eff} = \left\{ \frac{2m+1}{m+1} \int_0^d \left[\int_0^{x'} S(x)dx \right]^{m/(m+1)} dx' \right\}^{(m+1)/(2m+1)}. \tag{1b}$$

Here, d and $d_{\rm eff}$ are the actual and effective thicknesses of a charge transport layer, respectively, $S(x)$ is the spatial distribution of traps as a function of position x, and the exponent m is given by $(1 + 2\pi\sigma_{\rm t}^2/16k^2T^2)^{1/2}$ with $\sigma_{\rm t}$ the Gaussian width of the trap DOS, k the Boltzmann constant, and T the temperature.

The Kao and Hwang (K-H) model, represented by Eq. (1), provides insight into the electrical properties of organic devices in the presence of traps [15,25]. The K-H model suggests that the slope of the J-V characteristics $(m + 1)$ is determined by the energetic disorder of the traps $(\sigma_{\rm t})$, and under the condition of fixed $\sigma_{\rm t}$, the spatial disorder of the traps $[S(x)]$ modulates $d_{\rm eff}$ and determines the level of J at a given V. However, the K-H model can be only valid under limited conditions due to simplifying assumptions made in the derivation of Eq. (1): First, the model neglects the diffusion current, although it is found to dominate over the drift current in a low voltage regime in devices with Ohmic contacts [27]. Second, the trapped hole density $p_{\rm t}$ is exceedingly larger than the free hole density p for all x, i.e., $p_{\rm t}(x) \gg p(x) \approx 0$. Third, the electric field F at the anode/organic interface is assumed to be zero, i.e., $F(x = 0) = 0$. This assumption is not valid since p and $p_{\rm t}$ are present near the anode with high densities, leading to a nonzero and varying $F(0)$ with respect to the applied voltage. Due to these constraints not being met under our experimental conditions, we found that using Eq. (1) incurs a large deviation from the measured J-V data (see the Supplemental Material [28]).

Therefore, we developed a general trap-limited J-V model that incorporates the drift-diffusion current equation, Poisson's equation, the Fermi-Dirac statistics, which takes into account the Gaussian DOS for both the trap and hole-transport states, and an enhanced charge injection barrier due to charge trapping (*vide infra*). Our model is used to fit the J-V characteristics of our trap-containing HODs by calculating the electrical potential (V), free hole density (p), and trapped hole density ($p_{\rm t}$) as functions of position x in the HTL with a thickness of $d = 200$ nm. The hole traps are doped in a 5-nm-thick slab around the center point $x_{\rm t}$, i.e., in the range ($x_{\rm t}$–2.5 nm, $x_{\rm t} + 2.5$ nm) (refer to the Supplemental Material for more detailed information on our model [28]).

To solve the second-order differential equations for $V(x)$ and $p(x)$ in the model, we should define the B.C. for these two variables at $x = 0$ and $x = d$ at which hole injection and a hole extraction occur, respectively. The B.C. for V are given by $V(0) = V_{\rm a}$–$V_{\rm bi}$ and $V(d) = 0$, where $V_{\rm a}$ is the applied voltage and $V_{\rm bi}$ is the built-in potential. Here, $V_{\rm bi}$ can be viewed as the difference between the energy barriers for hole injection at $x = 0$ and extraction at $x = d$, denoted by $\phi_{\rm inj}$ and $\phi_{\rm ext}$, respectively, at a thermal equilibrium of $V_{\rm a} = 0$. Namely,

$$V_{\rm bi} = \phi_{\rm ext} - \phi_{\rm inj}(x_{\rm t},\ V_{\rm a} = 0), \tag{2a}$$

where

$$\phi_{\rm inj}(x_{\rm t},\ V_{\rm a}) = \Delta_0 + \Delta(x_{\rm t}) - l\sqrt{V_{\rm a}}. \tag{2b}$$

Equation (2b) indicates that the hole-injection barrier $(\phi_{\rm inj})$ can vary with respect to $x_{\rm t}$ and $V_{\rm a}$, as schematically described in Fig. 1. Here, Δ_0 in Fig. 1(a) represents the *intrinsic* band bending at equilibrium, which naturally arises if the HTL is in contact with a high work-function anode [27]. This can be understood as follows: In an instant after contact formation, the substantial density of holes diffuses from the anode into the HTL to align the Fermi level [12,13,29–31]. Then, the accumulated holes near the anode/HTL interface create an electric field towards the anode, resulting in the downward curvature of an electric potential (i.e., Δ_0). Note that the high work-function anode can render an *Ohmic-like* contact for efficient hole injection at the anode/HTL junction rather than a Schottky contact.

Now, in the presence of traps at $x = x_{\rm t}$ *near the anode* as shown in Fig. 1(b), the HTL band curves further downwards by $\Delta(x_{\rm t})$ due to the additional electric field that is exerted towards the anode by the trapped holes. On the other hand, the application of $V_{\rm a} > 0$ opposes the intrinsic (Δ_0) and *extrinsic* $[\Delta(x_{\rm t})]$ band bending so that $\phi_{\rm inj}$ is effectively reduced with respect to that at equilibrium (i.e., $V_{\rm a} = 0$) [see Fig. 1(c)]. We assumed that this bias-dependent barrier-lowering effect depends on the square root of $V_{\rm a}$ in Eq. (2b) inspired by the thermionic emission current model, where the current density is given by $J \propto \exp[-(\frac{\phi_{\rm inj}-\sqrt{qF/4\pi\varepsilon}}{kT})]$ with q the elementary charge and ε the permittivity. Here, $\phi_{\rm inj}$ is lowered by $\sqrt{q/4\pi\varepsilon d}\sqrt{V_{\rm a}}$ with an assumption of the constant electric field of $F = V_{\rm a}/d$ across the organic layer [11,32,33]. However, considering the space charge effect in our HOD, we replaced the constant prefactor $(\sqrt{q/4\pi\varepsilon d})$ with a scale factor of l that is set as a free parameter in our J-V model.

The B.C. for p can be given according to the Fermi-Dirac statistics for holes and the Gaussian DOS for the HTL as

$$p(x = 0, d) = \int_{-\infty}^{\infty} \frac{N_{\rm H}}{\sigma_{\rm H}\sqrt{2\pi}} \exp\left[-\frac{(E - E_0)^2}{2\sigma_{\rm H}^2}\right] \times \frac{1}{1 + \exp[(\phi_{\rm inj,ext} - E)/kT]} dE, \tag{3}$$

where E is an electronic state energy for holes, $N_{\rm H}$ is the total molecular density, E_0 is the center of the Gaussian DOS, and $\sigma_{\rm H}$ is the Gaussian width for the HTL molecules. Equation (3) indicates that the *injected* hole density $[p(0)]$ is a function of $\phi_{\rm inj}$ and hence it depends on $x_{\rm t}$ and $V_{\rm a}$. For example, extrinsic band bending $[\Delta(x_{\rm t})]$ caused by traps enhances the injection barrier $(\phi_{\rm inj})$ and thus reduces $p(0)$, whereas a positive $V_{\rm a}$ lowers $\phi_{\rm inj}$, thereby increasing $p(0)$. $p(0)$ determines the density of the free holes available in the HTL and hence the current density (J) in the HODs according to the drift-diffusion equation.

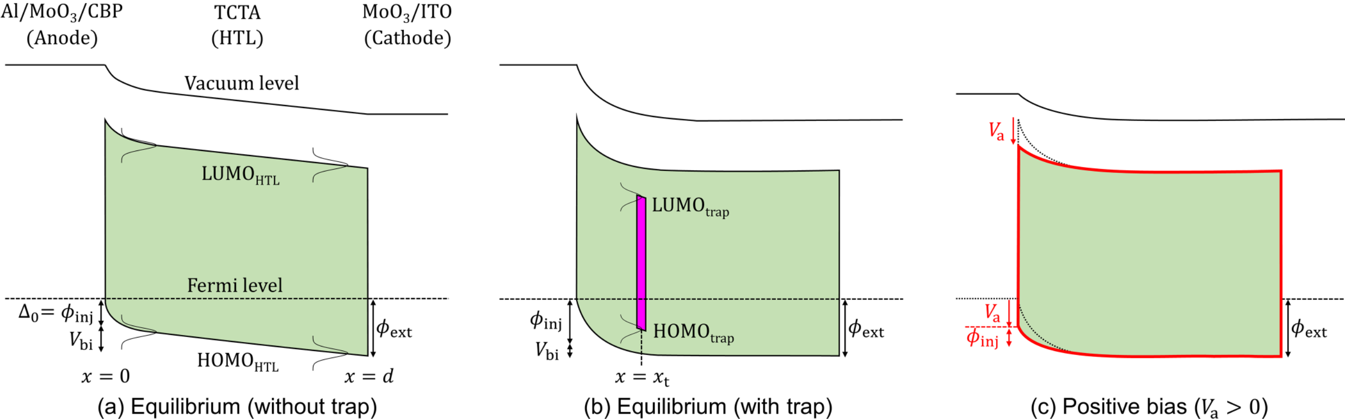

FIG. 1. Energy band diagrams for the HODs (a) at thermal equilibrium where *intrinsic* band bending (Δ_0) arises for the Fermi level alignment, effectively acting as a hole-injection barrier ($\phi_{\rm inj}$), (b) at equilibrium where additional *extrinsic* band bending occurs due to traps inserted near an anode at $x = x_{\rm t}$, further increasing $\phi_{\rm inj}$, (c) upon the application of a positive voltage ($V_{\rm a} > 0$) where band bending is mitigated, reducing $\phi_{\rm inj}$.

III. EXPERIMENT

The HODs were fabricated in an *inverted* structure: indium tin oxide (ITO)/10 nm MoO_3/200 nm tris(4-carbazoyl-9-ylphenyl)amine (TCTA)/3 nm 4,4′-bis(N-carbazolyl)biphenyl (CBP)/10 nm MoO_3/100 nm Al. Here, an anode with the sequence of Al, MoO_3, and CBP forms an *Ohmic-like* hole-injection contact with the TCTA HTL due to the CBP interlayer with its high ionization energy [34]. This allows us to focus on the hole transport properties in the HTL bulk by minimizing the injection-limited effects on the J-V characteristics. We chose 4,4′,4′′-tris[2-naphthyl(phenyl)amino]triphenylamine (2-TNATA) as a hole-trapping molecule due to its shallower highest occupied molecular orbital of HOMO $= -5.3 \pm 0.1$ eV vs -5.8 ± 0.1 eV for the TCTA HTL. This 0.5-eV difference eliminates the energetic overlap between the HTL and trap HOMOs, even considering the width of a Gaussian DOS ~0.1 eV for typical organics [31,34].

To ensure that trap molecules do not form filamentary paths for the *percolating* movement of the holes via the trap states and create complexity in analysis [19,24,35], we keep their concentration low at $\leqslant$1wt % [36,37]. 2-TNATA was doped at 1 wt % in a 5-nm-thick layer of the 200-nm-thick TCTA HTL, forming a *trap-containing slab* centered at $x = x_{\rm t}$ within the HTL. The "insertion" of the trap-containing slab at a desired position ($x_{\rm t}$) was done by sequentially depositing the partial HTL, slab, and then another partial HTL with their precisely controlled thickness. The vacuum pressure in the deposition chamber is kept below $\sim 5 \times 10^{-7}$ Torr to minimize the introduction of environmental impurities such as oxygen and water molecules into the HODs. The trap depth for 2-TNANA *in* TCTA was measured to be 0.5 ± 0.1 eV with ultraviolet photoelectron spectroscopy (UPS), precisely matching with the difference between their independently measured HOMO levels (see the Supplemental Material [28]).

We classified the HODs into two groups as shown in Fig. 2(a). The devices in "group 1" include a trap-containing slab centered at $x_{\rm t} = 0.2d$ up to $0.9d$ with an interval of $0.1d$, relatively far away from the anode. For the devices in "group 2," on the other hand, the slab is situated at a shorter distance of $x_{\rm t} = 0.025d$ to $0.1d$ to the anode with a shorter interval of $0.025d$. Group 2 was used to investigate strong trap-induced band bending near the anode with high precision.

IV. RESULTS AND DISCUSSION

Figures 2(b) and 2(c) show the J-V characteristics of a few select HODs from group 1 and group 2, respectively, along with that of a control device without traps (symbols: experimental data; solid and dotted lines: model fits). In contrast to the other devices in group 1 and group 2, the control device clearly exhibits a *trap-free* charge transport behavior consistent with the Mott-Gurney law (i.e., $J \propto V^2$) [38]. This indicates that the *intrinsic* or environmental traps that may be present in all HODs [24,39] do not act as hole traps due to the shallow HTL HOMO of -5.8 ± 0.1 eV (cf. -6.0 eV for water clusters; see Kotadiya *et al.* [39]). Thus, we confirmed that the only kind of hole traps active in the HODs is the *intentionally* introduced 2-TNATA molecule.

For the group 1 HODs, the J-V model with an assumption of $\Delta(x_{\rm t}) = 0$ shows a good agreement with the measured J-V data [Fig. 2(b)]. This indicates that the trap-induced band bending may be insignificant for the group 1 HODs whose traps are situated relatively far from their anode ($0.2d \leqslant x_{\rm t} \leqslant 0.9d$). However, for the group 2 HODs with the traps in proximity to the anode with $x_{\rm t} \lesssim 0.1d$, the J-V model with the same assumption [i.e., $\Delta(x_{\rm t}) = 0$] largely *overestimates* the actual J-V trend or the *conductivity* of the devices [dotted lines in Fig. 2(c)]. Furthermore, such a discrepancy progressively increases with decreasing $x_{\rm t}$. This model overestimation can be resolved by considering the mechanisms that can lessen the device conductivity: (i) the reduced hole mobility of the HTL or (ii) restricted hole injection into the HTL as $x_{\rm t}$ approaches the anode. While the former can be ruled out as it is not the case for group 1, the latter can result from *nonvanishing* trap-induced band bending [$\Delta(x_{\rm t}) \neq 0$ eV] [Eq. (2b)]. That is, the nonzero $\Delta(x_{\rm t})$ increases $\phi_{\rm inj}$ and hence concomitantly reduces $p(0)$, rendering the HODs to become

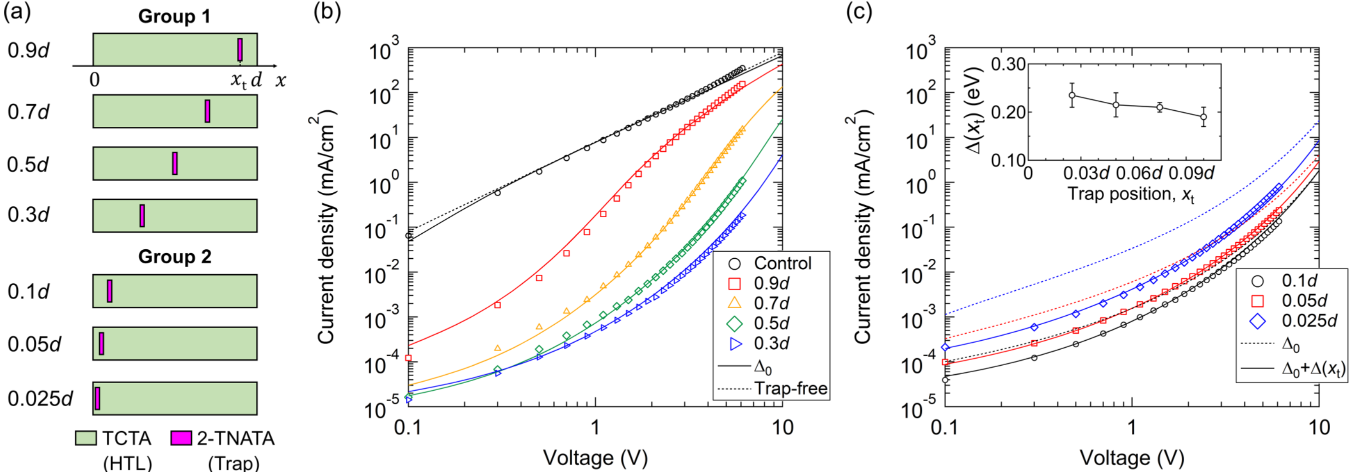

FIG. 2. (a) A few select HODs with traps inserted at different positions (x_t). The group 1 and group 2 HODs have the traps relatively far from ($0.2d \leqslant x_t \leqslant 0.9d$), and near ($x_t \leqslant 0.1d$), their anode, respectively, with d the thickness of the HTL. (b) The J-V characteristics for the group 1 HODs and the control device without traps [dotted line: J-V model following the Mott-Gurney law; solid lines: our J-V model only assuming intrinsic band bending (Δ_0); symbols: experimental data]. (c) The J-V characteristics for the group 2 HODs [dotted and solid lines: our J-V models with the assumptions of $\Delta(x_t) = 0$ and $\Delta(x_t) > 0$, respectively]. The inset shows the nonzero $\Delta(x_t)$ values with respect to x_t for the group 2 HODs.

resistive. The J-V model with the *revised* $\Delta(x_t)$ values can precisely fit the data for the group 2 HODs [solid lines in Fig. 2(c)].

Note that $\Delta(x_t)$ increases with decreasing x_t only if the traps are in close proximity to the anode ($x_t \lesssim 0.1d$), but otherwise $\Delta(x_t) \approx 0$ eV ($x_t \geqslant 0.2d$). This is because the trapped holes nearer the anode exert a stronger electric field towards the anode, further inducing downwards band bending (see the Supplemental Material for verification [28,40]). Note also that because the density of trapped holes (p_t) increases with the applied electric field or voltage (V_a), so does the nonzero $\Delta(x_t)$ for $x_t \lesssim 0.1d$, which arises due to p_t in the first place. However, the variation of p_t vs V_a is small despite the addition of free holes (p) due to the much larger density of $p_t > 10^{24}\,\mathrm{m^{-3}}$ vs $p \approx 10^{18} \sim 10^{23}\,\mathrm{m^{-3}}$ across the HODs (*vide infra*), which is attributed to the favorable energy level for the trap states (i.e., $E_t = 0.5 \pm 0.1$ eV) to readily capture a majority of free holes even at a very low V_a. This leads to the negligible V_a-dependence of $\Delta(x_t)$.

On the other hand, the band bending can be mitigated by a positive applied bias ($V_a > 0$) [see Fig. 1(c) and Eq. (2b)]. To account for this bias-dependent barrier lowering for HODs, the fitting parameter l in Eq. (2b) was obtained to be 0.09, which is nearly twice the prefactor $\sqrt{q/4\pi\varepsilon d} \approx 0.05$ for the thermionic emission model with the assumption of a constant electric field. This discrepancy may be attributed to the *space charge effect* in our HODs, one of the fundamental assumptions in our model (see the Supplemental Material [28]) that leads to the nonuniform electric field across the devices (*vide infra*). Another possible explanation can be given in terms of an energy broadening effect in the organic layer at a metal-organic interface. The energy broadening originates from the disorder of interfacial dipoles formed between the metal and organic [11]; however, upon the application of the positive bias, such *disordered* dipoles would tend to align in the direction of the electric field. This, as a result, can reduce the energy broadening of the organic layer with a *narrowed* Gaussian DOS such that charge injection from the metal into the organic layer may be facilitated.

To investigate the overall trend of the J-V characteristics with respect to the trap position, we present a contour map of log J as functions of x_t and V_a in Fig. 3(a). The black contour line at $J_0 = 0.01\,\mathrm{mA/cm^2}$ shows two trends: (1) the required V_a to attain J_0 increases with decreasing x_t from $0.9d$ to $0.2d$ (i.e., the HODs become resistive); (2) for $x_t \lesssim 0.2d$, the trend is reversed (i.e., the HODs become conductive). To understand this, we plot in Fig. 3(b) the distributions of free (p) and trapped holes (p_t) along with the electric field profile (F) at $J_0 = 0.01\,\mathrm{mA/cm^2}$ for the three selected HODs with traps inserted at $x_t = 0.05d$, $0.3d$, and $0.5d$, respectively. The commonality for these devices is that p sharply drops near the trap-inserted position at $x = x_t$ due to strong charge localization, manifested also as a large local density of p_t therein. In the case of $x_t = 0.5d$, for example, the proportion of trapped holes vs total holes, $\int_0^d p_t(x)dx / \int_0^d [p(x) + p_t(x)]dx$, is approximately 40%. This is remarkable in that only 1 wt% of the traps within a 5-nm-thick slab (i.e., 2.5% of the entire thickness) can localize nearly a half of the total available holes. It is the result of the trap depth of $E_t = 0.5 \pm 0.1$ eV being deep enough to readily and exothermically attract holes from the transport energy level.

The remaining free holes (p) between the trap-containing slab at $x = x_t$ and the cathode at $x = d$ are nearly negligible, for which p in this region is smaller by at least ~ 3 orders of magnitude than the injected hole density [$p(0)$]. As a result, the electric field in the direction of the cathode ($F > 0$) surges at which a large local p_t arises near $x = x_t$, but it flattens out in the region of $x_t \lesssim x \leqslant d$ due to the scarcity of overall holes therein according to $F(x) = F(0) + \int_0^x \frac{q}{\varepsilon}[p(x') + p_t(x')]dx'$ [Fig. 3(b)]. Therefore, as x_t approaches the anode more, the width of this flattened or *constant-electric field* region at $x_t \lesssim x \leqslant d$ becomes wider. This leads to the higher V_a to maintain a given J_0 according to $V_a \approx -\int_d^0 F(x')dx'$, indicating that the

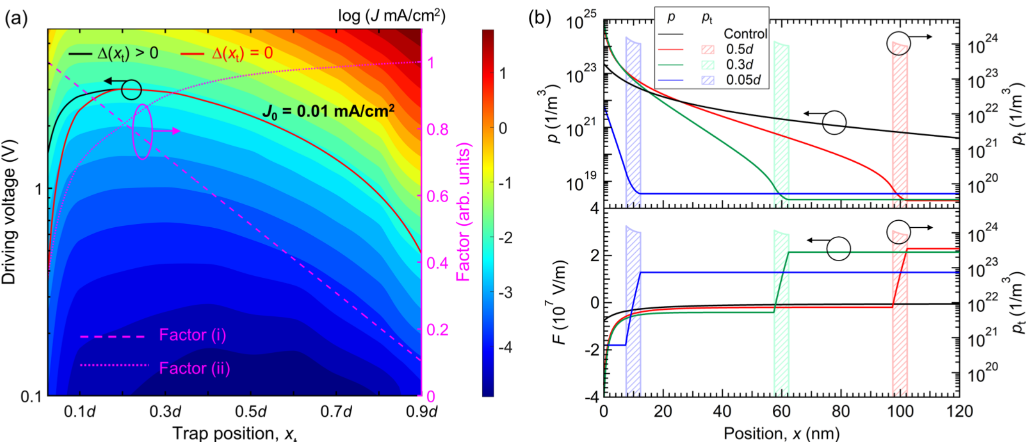

FIG. 3. (a) Contour plot of the current density of the HODs with respect to trap position (x_t) and driving voltage (V_a). Solid lines represent a required V_a to attain $J_0 = 0.01\ \mathrm{mA/cm^2}$ for the HODs with traps at $x = x_t$, calculated using the J-V model with and without considering the effect of $\Delta(x_t)$. Dashed and dotted lines represent the relative contributions of the width of the constant-F region [factor (i)] and the negative shift of $F(x)$ [factor (ii)], respectively, to the contour line with respect to x_t. (b) (upper panel) The profile of the free hole density (p; solid line), trapped hole density (p_t; diagonal pattern), and (lower panel) electric field (F; solid line) for a few select HODs with traps inserted at $x_t = 0.05d$, $0.3d$, and $0.5d$, all of which are calculated at $J_0 = 0.01\ \mathrm{mA/cm^2}$.

HODs become more resistive with decreasing x_t, as is found in trend (1). In short, the free holes available in the devices become more deficient as they are captured by the traps nearer to the anode and this leads to the reduced device conductivity, i.e., requiring the higher V_a to attain J_0, as indicated by the decreasing slope of the J-V curves for the group 1 HODs with decreasing x_t [Fig. 2(b)].

While the same effect also holds true for the case with $x_t \lesssim 0.2d$, it is overwhelmed by a *counterbalancing* factor that renders the HODs to become conductive with decreasing x_t, i.e., trend (2)—an entire negative shift of the $F(x)$ that occurs with decreasing x_t such that the magnitude of $F(x) > 0$ in the direction of the cathode progressively reduces (i.e., at $x_t \lesssim x \leqslant d$), whereas $F(x) < 0$ in the direction of the anode is further intensified (i.e., at $0 \leqslant x \lesssim x_t$). This can be understood in terms of the relative distance between the trapped charges [$p_t(x_t)$] and the respective electrodes, which modulates the magnitude of $F(x)$ according to *the method of images*. The observed relationship of $F(x)$ vs x_t can be more clearly shown by solving the Poisson's equation with $p_t(x_t)$ with a fixed density, excluding the influence of the free charges [i.e., $p(x) = 0$] without loss of generality (see the Supplemental Material [28]).

In summary, the turning point of the device conductivity curve (i.e., the contour line at J_0) is determined by the interplay of three factors: (i) the broadening of the width of the constant-F region, (ii) the negative shift of the entire $F(x)$ profile, and (iii) the trap-induced bend bending [$\Delta(x_t)$]. Factors (i) and (iii) render the HODs resistive, whereas factor (ii) exerts the opposite effect. Figure 3(a) shows the relative contribution of the individual factors to the device conductivity with respect to x_t. Factor (i), represented by a dashed line, is dominant in the range $0.2d \lesssim x_t \leqslant 0.9d$, whereas factors (ii) and (iii) become activated with decreasing $x_t \lesssim 0.2d$; however, even though the effect of factor (iii), rendering the HODs resistive, is present [see the difference between black and red solid lines assuming $\Delta(x_t) > 0$ and $\Delta(x_t) = 0$, respectively], factor (ii), represented by a dotted line, is so dominant that the HODs become conductive after all, manifested as the turning point of the contour line in Fig. 3(a).

V. CONCLUSIONS

We investigated the effects of traps on the electrical characteristics of unipolar organic devices by varying the position of the traps in the devices. We found that the traps near an anode induce strong band bending of the organic layer, thereby hindering charge injection into the device. In addition, the position of the traps critically determines the distribution of the free and trapped charges, the electric field, and hence the conductivity of the device. Note that our analysis on organic devices could be easily transferrable to any type of device based on amorphous semiconductors. This is because although the material composition for amorphous semiconductor devices is different, the governing principle of charge dynamics, electronic states arising due to the structural disorder, and their variation due to the presence of traps can be common in a broad sense. Our findings indicate that for amorphous semiconductor devices in which environmental or degradation-induced traps are normally found, a slight spatial disorder of the traps even with a minute amount can largely modulate the entire electrical properties of the devices. It is therefore imperative to figure out what kinds of traps are present in devices in the first place and then the effects of such traps with their originating position and distribution, as was proposed in this study.

ACKNOWLEDGMENTS

This work was supported by the New Faculty Startup Fund from Seoul National University, the Industrial Strategic Technology Development program funded by the Ministry of Trade, Industry & Energy (MOTIE, Korea) (Grant No. 20011059), the National Research Foundation

of Korea (NRF) grant funded by the Korean government (MSIT) (Grants No. 2020R1C1C1008659 and No. 2021R1A2C1012754), and Samsung Display. The UPS data were measured using the equipment in Multidimensional Materials Research Center at Kyung Hee University (Grant No. 2021R1A6C101A437).

[1] H. Sirringhaus, Adv. Mater. **17**, 2411 (2005).
[2] R. A. Street, Phys. Rev. B **84**, 075208 (2011).
[3] L. Burtone, J. Fischer, K. Leo, and M. Riede, Phys. Rev. B **87**, 045432 (2013).
[4] G. A. H. Wetzelaer, M. Scheepers, A. M. Sempere, C. Momblona, J. Ávila, and H. J. Bolink, Adv. Mater **27**, 1837 (2015).
[5] J. M. Pietryga, Y. S. Park, J. H. Lim, A. F. Fidler, W. K. Bae, S. Brovelli, and V. I. Klimov, Chem. Rev. **116**, 10513 (2016).
[6] J. Lee, C. Jeong, T. Batagoda, C. Coburn, M. E. Thompson, and S. R. Forrest, Nat. Commun. **8**, 15566 (2017).
[7] H. F. Haneef, A. M. Zeidell, and O. D. Jurchescu, J. Mater. Chem. C **8**, 759 (2020).
[8] S. Zeiske, O. J. Sandberg, N. Zarrabi, W. Li, P. Meredith, and A. Armin, Nat. Commun. **12**, 3603 (2021).
[9] G. A. H. Wetzelaer, M. Kuik, H. T. Nicolai, and P. W. M. Blom, Phys. Rev. B **83**, 165204 (2011).
[10] B. Sim, J. S. Kim, H. Bae, S. Nam, E. Kwon, J. W. Kim, H. Y. Cho, S. Kim, and J. J. Kim, Phys. Rev. Appl. **14**, 024002 (2020).
[11] M. A. Baldo and S. R. Forrest, Phys. Rev. B **64**, 085201 (2001).
[12] I. Lange, J. C. Blakesley, J. Frisch, A. Vollmer, N. Koch, and D. Neher, Phys. Rev. Lett. **106**, 216402 (2011).
[13] M. Oehzelt, N. Koch, and G. Heimel, Nat. Commun. **5**, 4174 (2014).
[14] J. Bonham, Aust. J. Chem. **26**, 927 (1973).
[15] H. T. Nicolai, M. M. Mandoc, and P. W. M. Blom, Phys. Rev. B **83**, 195204 (2011).
[16] B. H. Cumpston and K. F. Jensen, Appl. Phys. Lett. **69**, 3941 (1996).
[17] S. T. Lee, Z. Q. Gao, and L. S. Hung, Appl. Phys. Lett. **75**, 1404 (1999).
[18] S. Scholz, D. Kondakov, B. Lussem, and K. Leo, Chem. Rev. **115**, 8449 (2015).
[19] K. Yang, S. Nam, J. Kim, E. S. Kwon, Y. Jung, H. Choi, J. W. Kim, and J. Lee, Adv. Funct. Mater. **32**, 2108595 (2022).
[20] N. C. Erickson and R. J. Holmes, Adv. Funct. Mater. **24**, 6074 (2014).
[21] Y. F. Zhang, J. Lee, and S. R. Forrest, Nat. Commun. **5**, 5008 (2014).
[22] J. Lee, H. F. Chen, T. Batagoda, C. Coburn, P. I. Djurovich, M. E. Thompson, and S. R. Forrest, Nat. Mater. **15**, 92 (2016).
[23] B. van der Zee, Y. Li, G.-J. A. H. Wetzelaer, and P. W. M. Blom, Phys. Rev. Appl. **18**, 064002 (2022).
[24] D. Ko and J. Lee, SID. Symp. Dig. Tech. Pap. **51**, 2121 (2020).
[25] W. Hwang and K. C. Kao, Solid State Electron. **19**, 1045 (1976).
[26] K. C. Kao and W. Hwang, *Electrical Transport in Solids* (Oxford, Pergamon, 1981).
[27] P. de Bruyn, A. H. P. van Rest, G. A. H. Wetzelaer, D. M. de Leeuw, and P. W. M. Blom, Phys. Rev. Lett. **111**, 186801 (2013).
[28] See Supplemental Material at http://link.aps.org/supplemental/10.1103/PhysRevB.107.165204 for J-V model, UPS measurement, and the effect of the trap position on the electric field.
[29] J. C. Blakesley and N. C. Greenham, J. Appl. Phys. **106**, 034507 (2009).
[30] S. Olthof, R. Meerheim, M. Schober, and K. Leo, Phys. Rev. B **79**, 245308 (2009).
[31] M. T. Greiner, M. G. Helander, W. M. Tang, Z. B. Wang, J. Qiu, and Z. H. Lu, Nat. Mater. **11**, 76 (2012).
[32] V. I. Arkhipov, E. V. Emelianova, Y. H. Tak, and H. Bassler, J. Appl. Phys. **84**, 848 (1998).
[33] J. C. Scott and G. G. Malliaras, Chem. Phys. Lett. **299**, 115 (1999).
[34] N. B. Kotadiya, H. Lu, A. Mondal, Y. Ie, D. Andrienko, P. W. M. Blom, and G. A. H. Wetzelaer, Nat. Mater. **17**, 329 (2018).
[35] C.-H. Lee, J.-H. Lee, K.-H. Kim, and J.-J. Kim, Adv. Funct. Mater. **28**, 1800001 (2018).
[36] I. I. Fishchuk, A. K. Kadashchuk, A. Vakhnin, Y. Korosko, H. Bassler, B. Souharce, and U. Scherf, Phys. Rev. B **73**, 115210 (2006).
[37] S. Sanderson, B. Philippa, G. Vamvounis, P. L. Burn, and R. D. White, J. Chem. Phys. **150**, 094110 (2019).
[38] N. F. Mott and R. W. Gurney, *Electronic Processes in Ionic Crystals* (Dover, New York, 1964).
[39] N. B. Kotadiya, A. Mondal, P. W. M. Blom, D. Andrienko, and G. A. H. Wetzelaer, Nat. Mater. **18**, 1182 (2019).
[40] J. H. Kim, J. Seo, D. G. Kwon, J. A. Hong, J. Hwang, H. K. Choi, J. Moon, J. I. Lee, D. Y. Jung, S. Y. Choi, and Y. Park, Carbon **79**, 623 (2014).